J|A|C|S
ARTICLES

Published on Web 05/22/2009

Shear- and UV-Induced Fluorescence Switching in Stilbenic π-Dimer Crystals Powered by Reversible [2 + 2] Cycloaddition

Jong Won Chung,[†] Youngmin You,[†] Hyun Sue Huh,[‡] Byeong-Kwan An,[†] Seong-Jun Yoon,[†] Se Hun Kim,[†] Soon W. Lee,[‡] and Soo Young Park*,[†]

Center for Supra molecular Optoelectronics Materials and Department of Materials Science and Engineering, ENG445, Seoul National University, San 56-1, Shilim-dong, Kwanak-ku, Seoul 151-744, Korea, and Department of Chemistry, Sungkyunkwan University Natural Science Campus, 32308 Suwon 440-746, Korea

Received February 2, 2009; E-mail: parksy@snu.ac.kr

Abstract: We have designed and synthesized asymmetric cyano-stilbene derivatives containing trifluoromethyl ($-CF_3$) substituents with the aim of producing tightly packed π-dimer systems that as crystals exhibit reversible [2 + 2] cycloaddition with characteristic fluorescence modulation. (*Z*)-3-(3′,5′-Bis(trifluoromethyl)biphenyl-4-yl)-2-(4′-(trifluoromethyl)biphenyl-4-yl)acrylonitrile (CN(L)-TrFMBE) and its derivatives were found to form antiparallel π-dimer stacks in crystals due to their specific intermolecular interactions, including C−F···H and C−F···π interactions. The CN(L)-TrFMBE π-dimer crystals (and powder) are not at all fluorescent initially but switch to a highly fluorescent state (Φ_{PL} = 24%) when an external shear-strain and/or prolonged UV (365 nm) irradiation is applied. Our experimental and theoretical investigations show that the fluorescence modulation in this particular system is due to the external and/or internal (in the case of UV irradiation) shear-induced lateral displacement of the π-dimer molecular pair, which effectively turns the fluorescence emission on at the cost of frustrated [2 + 2] cycloaddition. Further, the fluorescence 'off' state can be restored by thermal annealing, which regenerates the tightly packed π-dimer by reverse displacement together with the thermal dissociation of the [2 + 2] cycloaddition product. This system provides a very rare example of high-contrast reversible fluorescence switching that is driven by a change in the molecular packing mode in the solid state, which enables piezochromic and photochromic responses.

Introduction

The photophysical properties of a given molecular system in the condensed phase, such as fluorescence emission and vibrational relaxation, undergo significant variation according to the mode of molecular stacking, because intermolecular interactions invariably alter photophysical processes. Therefore, understanding and controlling molecular stacking modes and the consequent intermolecular interactions are very important for obtaining solid-state material systems with the desired chemical and physical properties.[1] In this respect, it is essential to establish a molecular level understanding of the correlations between molecular structure, stacking modes, and photophysical properties.[2−4]

Solid-state organic reactions have attracted extensive attention because of their various interesting features that are related to molecular stacking events, such as high regio- and stereoselectivity and lattice-controlled reactions, and because they can be carried out in the absence of solvents or catalysts, and requiring no isolation or purification of the desired products.[5] In particular, topochemical [2 + 2] cycloaddition reactions are highly stacking-mode specific in generating photoadducts.[5−8] Bringing

[†] Seoul National University.
[‡] Sungkyunkwan University Natural Science Campus.

(1) (a) Been, H.; Weller, A. *Organic Molecular Photophysics*; Wiley: New York, 1975; Vol. 2. (b) Mimura, T.; Itoh, M. *J. Am. Chem. Soc.* **1976**, *98*, 1091–1095. (c) DeSchryver, F. *Adv. Photochem.* **1977**, *10*, 359. (d) Bera, R. N.; Cumpstey, N.; Burn, P. L.; Samuel, I. D. W. *Adv. Func. Mat.* **2007**, *17*, 1149–1152. (e) Lu, W.; Chan, M. C. W.; Zhu, N. Y.; Che, C. M.; Li, C. N.; Hui, Z. *J. Am. Chem. Soc.* **2004**, *126*, 7639–7651.
(2) (a) Förster, T. *Angew. Chem., Int. Ed.* **1969**, *8*, 333–343. (b) Weller, A. *Pure Appl. Chem.* **1968**, *16*, 115. (c) Birks, J. B. *In Photophysics of Aromatic Molecules*; Wiley: London, 1970.
(3) (a) Crenshaw, B. R.; Weder, C. *Chem. Mater.* **2003**, *15*, 4717–4724. (b) Ikeda, M.; Takeuchi, M.; Shinkai, S. *Chem. Commun.* **2003**, 1354–1355. (c) Langhals, H.; Potrawa, T.; Noth, H.; Linti, G. *Angew. Chem., Int. Ed.* **1989**, *28*, 478–480. (d) Oyamada, T.; Akiyama, S.; Yahiro, M.; Saigou, M.; Shiro, M.; Sasabe, H.; Adachi, C. *Chem. Phys. Lett.* **2006**, *421*, 295–299.
(4) (a) Davis, R.; Kumar, N. S. S.; Abraham, S.; Suresh, C. H.; Rath, N. P.; Tamaoki, N.; Das, S. *J. Phys. Chem. C* **2008**, *112*, 2137–2146. (b) Kumar, N. S. S.; Varghese, S.; Rath, N. P.; Das, S. *J. Phys. Chem. C* **2008**, *112*, 8429–8437. (c) MacGillivray, L. R. *Nature* **2008**, *451*, 897–898. (d) Desiraju, G. R. *Angew. Chem., Int. Ed.* **2007**, *46*, 8342–8356. (e) Dong, J.; Solntsev, K. M.; Tolbert, L. M. *J. Am. Chem. Soc.* **2009**, *131*, 662–670.
(5) (a) Ramamurthy, V.; Venkatesan, K. *Chem. Rev.* **1987**, *87*, 433–481. (b) Hasegawa, M. *Pure. Appl. Chem.* **1986**, *58*, 1179–1188. (c) Hasegawa, T.; Ikeda, K.; Yamazaki, Y. *J. Chem. Soc. Perkin Trans. 1* **2001**, 3025–3028.
(6) (a) Cohen, M. D.; Schmidt, G. M. J. *J. Chem. Soc.* **1964**, 1996–2000. (b) Cohen, M. D.; Schmidt, G. M. J. J.; Sonntag, F. I. *J. Chem. Soc.* **1964**, 2000–2013. (c) Schmidt, G. M. J. *J. Chem. Soc.* **1964**, 2014–2021. (d) Schmidt, G. M. J. *Pure Appl. Chem.* **1971**, *27*, 647.
(7) (a) Amato, M. E.; Musumarra, G.; Scarlata, G.; Lamba, D.; Spagna, R. *J. Crystallogr. Spectrosc. Res.* **1989**, *19*, 791–808. (b) Wegner, G. *Pure Appl. Chem.* **1977**, *49*, 443. (c) Hoyer, T.; Tuszynski, W.; Lienau, C. *Chem. Phys. Lett.* **2007**, *443*, 107–112. (d) Ito, Y.; Borecka, B.; Olovsson, G.; Trotter, J.; Scheffer, J. R. *Tetrahedron Lett.* **1995**, *36*, 6087–6090.

two π-bonds into close proximity with the correct orientation is a key step in the promotion of [2 + 2] cycloaddition reactions with a high reaction rate in a regio- and stereoselective manner. For these reactions to occur, the olefin units must be aligned in parallel and the distance between the two reacting molecules must be small (ca. <4.2 Å), forming a *π-dimer*.[6] To promote favorable stacking interactions between small organic molecules, linear templates[9] and coordination-driven self-assembly[10] have been used. Molecular structural factors for predicting stacking interactions have also been extensively investigated.[11−16] In particular, specific functional groups and/or intermolecular interactions have been found to induce tight stacking in crystalline arrangements. For example, chloro-,[11] fluoro-,[12,18] and alkoxyaryl substituents,[13] as well as electron donor−acceptor[14] and hydrogen bonding interactions,[15] have been used to induce the tight dimer stacking of olefin molecules in crystals for [2 + 2] cycloaddition. A π-conjugated molecule with a fluorine-containing aromatic ring has been reported to favor either antiparallel molecular stacking[16] or offset stacking[17] rather than the parallel cofacial stacking that is very common in π-conjugated molecular systems. This unique stacking tendency is attributed to its specific intermolecular interactions, including C−F···H−C and C−F···π, which are the noncovalent interactions of the highly electronegative fluorine atoms in the CF_3 units with either the hydrogen atoms or π-orbitals in the phenyl rings of the neighboring molecules.[18]

It is also known that fluorescence emission is altered remarkably by molecular stacking interactions, such as in the generation of additional emissions from *H*- and *J*-dimer/aggregates,[19] as well as in excimer or exciplex emissions.[2,3] We have recently demonstrated that the formation of appropriate molecular stacking can turn on the fluorescence emission from structurally twisted and thus nonfluorescent molecular materials such as 1-cyano-*trans*-1,2-bis-(4′-methylbiphenyl)ethylene (CN-MBE).[20] This "aggregation-induced enhanced emission" (AIEE) is of great practical importance because of its solid state applications, particularly in nano-optoelectronic devices.[21] Our extensive studies with various CN-MBE derivatives have shown that *J*-type stacking combined with molecular planarization is responsible for the enhanced emission and the fluorescence turn-on.[20,22−26] This observation is consistent with the theoretical prediction of Kasha[27] that the *J*-aggregate, in contrast to the more common *H*-aggregate, preferentially reduces nonradiative decays in the highly interacting solid state and thus allows red-shifted and significantly enhanced fluorescence emission. Due to their strong tendency to form aggregates, AIEE molecules are easily self-assembled into highly fluorescent nanoparticles[20] and nanowires.[22] Moreover, fluorescent photochromic nanoparticles,[23] the array patterning of fluorescent nanoparticles,[24] a fluorescent switchable smart gel,[25] and a fluorescent superhydrophobic surface[26] produced *via* the structural derivatization of cyanostilbene-based AIEE molecules have also been reported.

In the course of exploring the effects of various substituents on the AIEE properties of CN-MBE derivatives, we observed shear- and/or UV-induced fluorescence emission from two novel AIEE molecules (**1** and **2**; see Scheme 1 for their structures) that have asymmetric substitutions of highly electron-withdrawing CF_3 units. The reference AIEE compound CN-TFMBE has symmetric CF_3 substituents (**3**; see Scheme 1 for its structure) and exhibits different behavior, which suggests that asymmetric substitution induces a stacking mode that is very different from *J*-type stacking. In this comprehensive structural and photophysical study, we were able to determine that the antiparallel

(8) (a) Tanaka, K.; Toda, F. *Chem. Rev.* **2000**, *100*, 1025–1074. (b) Singh, A. K.; Krishna, T. S. R. *J. Phys. Chem. A* **1997**, *101*, 3066–3069. (c) Bertmer, M.; Nieuwendaal, R. C.; Barnes, A. B.; Hayes, S. E. *J. Phys. Chem. B* **2006**, *110*, 6270–6273. (d) Nagarathinam, M.; Peedikakkal, A. M. P.; Vittal, J. J. *Chem. Commun.* **2008**, 5277–5288.

(9) (a) MacGillivray, L. R.; Reid, J. L.; Ripmeester, J. A. *J. Am. Chem. Soc.* **2000**, *122*, 7817–7818. (b) MacGillivray, L. R. *J. Org. Chem.* **2008**, *73*, 3311–3317. (c) Bocar, D. K.; Papaefstathiou, G. S.; Hamilton, T. D.; Chu, Q. L.; Georgiev, I. G.; MaeGillivray, L. R. *Eur. J. Inorg. Chem.* **2007**, 4559–4568. (d) Papaefstathiou, G. S.; Zhong, Z.; Geng, L.; MacGillivray, L. R. *J. Am. Chem. Soc.* **2004**, *126*, 9158–9159.

(10) (a) Michaelides, A.; Skoulika, S.; Siskos, M. G. *Chem. Commun.* **2004**, 2418–2419. (b) Toh, N. L.; Nagarathinam, M.; Vittal, J. J. *Angew. Chem., Int. Ed.* **2005**, *44*, 2237–2241. (c) Papaefstathiou, G. S.; Zhong, Z. M.; Geng, L.; MacGillivray, L. R. *J. Am. Chem. Soc.* **2004**, *126*, 9158–9159. (d) Nagarathinam, M.; Vittal, J. J. *Chem. Commun.* **2008**, 438–440.

(11) (a) Matsumoto, A.; Tanaka, T.; Tsubouchi, T.; Tashiro, K.; Saragai, S.; Nakamoto, S. *J. Am. Chem. Soc.* **2002**, *124*, 8891–8902.

(12) (a) Caronna, T.; Liantonio, R.; Logothetis, T. A.; Metrangolo, P.; Pilati, T.; Resnati, G. *J. Am. Chem. Soc.* **2004**, *126*, 4500–4501. (b) Mori, Y.; Matsumoto, A. *Cryst. Growth Des.* **2007**, *7*, 377–385.

(13) Gnanaguru, K.; Ramasubbu, N.; Venkatesan, K.; Ramamurthy, V. *J. Org. Chem.* **1985**, *50*, 2337–2346.

(14) (a) Devic, T.; Batail, P.; Avarvari, N. *Chem. Commun.* **2004**, 153 8–1539. (b) Beckers, E. H. A.; Meskers, S. C J.; Schenning, A. P. H. J.; Chen, Z. J.; Wurthner, F.; Marsal, P.; Beljonne, D.; Cornil, J.; Janssen, R. A. J. *J. Am. Chem. Soc.* **2006**, *128*, 649–657.

(15) (a) Khan, M.; Brunklaus, G.; Enkelmann, V.; Spiess, H. W. *J. Am. Chem. Soc.* **2008**, *130*, 1741–1748. (b) Darcos, V.; Griffith, K.; Sallenave, X.; Desvergne, J. P.; Guyard-Duhayon, C.; Hasenknopf, B.; Bassani, D. M. *Photochem. Photobiol. Sci.* **2003**, *2*, 1152–1161.

(16) (a) Coates, G. W.; Dunn, A. R.; Henling, L. M.; Ziller, J. W.; Lobkovsky, E. B.; Grubbs, R. H. *J. Am. Chem. Soc.* **1998**, *120*, 3641–3649. (b) Vishnumurthy, K.; Row, T. N. G.; Venkatesan, K. *Photochem. Photobiol. Sci.* **2002**, *1*, 427–430. (c) Yamada, S. J.; Uematsu, N.; Yamashita, K. *J. Am. Chem. Soc.* **2007**, *129*, 12100–12101.

(17) (a) Liu, J.; Wendt, N. L.; Boarman, K. J. *Org. Lett.* **2005**, *7*, 1007–1010. (b) Liu, J.; Boarman, K. J. *Chem. Commun.* **2005**, 340–341.

(18) (a) Boitsov, S.; Songstad, J.; Tornroos, K. W. *Acta Crystallogr. C* **2002**, *58*, o66−o68. (b) Shimoni, L.; Carrell, H. L.; Glusker, J. P.; Coombs, M. M. *J. Am. Chem. Soc.* **1994**, *116*, 8162–8168. (c) Rashkin, M. J.; Waters, M. L. *J. Am. Chem. Soc.* **2002**, *124*, 1860–1861. (d) Emmerling, F.; Orgzall, I.; Dietzel, B.; Schulz, B. W.; Reck, G.; Schulz, B. *J. Mol. Struct.* **2007**, *832*, 124–131. (e) Xu, R.; Schweizer, W. B.; Frauenrath, H. *J. Am. Chem. Soc.* **2008**, *130*, 11437–11445.

(19) (a) Glass, W. A.; Varma, M. N. In *Physical and Chemical Mechanism in Molecular Radiation Biology*; Plenum Press: New York, 1991. (b) Rae, E. G. M.; Kasha, M. The Molecular Exciton Model. In *Physical Processes in Radiation Biology*; Academic Press: New York, 1964. (c) Mishra, A.; Behera, R. K.; Behera, P. K.; Mishra, B. K.; Behera, G. B. *Chem. Rev.* **2000**, *100*, 1973–2011. (d) Harrison, W. J.; Mateer, D. L.; Tiddy, G. J. T. *J. Phys. Chem.* **1996**, *100*, 2310–2321.

(20) An, B.-K.; Kwon, S. K.; Jung, S. D.; Park, S. Y. *J. Am. Chem. Soc.* **2002**, *124*, 14410–14415.

(21) Guo, X. F.; Zhang, D. Q.; Zhu, D. B. *Adv. Mater.* **2004**, *16*, 125–130.

(22) (a) An, B.-K.; Lee, D. S.; Lee, J. S.; Park, Y. S.; Song, H. S.; Park, S. Y. *J. Am. Chem. Soc.* **2004**, *126*, 10232–10233. (b) An, B.-K.; Gihm, S. H.; Chung, J. W.; Park, C. R.; Kwon, S.-K.; Park, S. Y. *J. Am. Chem. Soc.* **2009**, *131*, 3950–3957.

(23) Lim, S. J.; An, B.-K.; Jung, S. D.; Chung, M. A.; Park, S. Y. *Angew. Chem., Int. Ed.* **2004**, *43*, 6346–6350.

(24) An, B.-K.; Kwon, S. K.; Park, S. Y. *Angew. Chem., Int. Ed.* **2007**, *46*, 1978–1982.

(25) Chung, J. W.; An, B.-K.; Park, S. Y. *Chem. Mater.* **2008**, *20*, 6750–6755.

(26) Chung, J. W.; An, B.-K.; Kim, J. W.; Kim, J. J.; Park, S. Y. *Chem. Commun.* **2008**, 2998–3000.

(27) Kasha, M. *Rev. Mod. Phys.* **1959**, *31*, 162–169.

(28) (a) Samori, P.; Francke, V.; Enkelmann, V.; Mullen, K.; Rabe, J. P. *Chem. Mater.* **2003**, *15*, 1032–1039. (b) Zhang, H. Y.; Zhang, Z. L.; Ye, K. Q.; Zhang, J. Y.; Wang, Y. *Adv. Mater.* **2006**, *18*, 2369–2372. (c) Miao, Q.; Chi, X. L.; Xiao, S. X.; Zeis, R.; Lefenfeld, M.; Siegrist, T.; Steigerwald, M. L.; Nuckolls, C. *J. Am. Chem. Soc.* **2006**, *128*, 1340–1345. (d) Elmahdy, M. M.; Dou, X.; Moncleshki, M.; Floudas, G.; Butt, H. J.; Spiess, H. W.; Mullen, K. *J. Am. Chem. Soc.* **2008**, *130*, 5311–5319. (e) Sanz, N.; Baldeck, P. L.; Nicoud, J. F.; Le Fur, Y.; Ibanez, A. *Solid State Sci.* **2001**, *3*, 867–875.

Scheme 1. Molecular Structures of Asymmetric (**1** and **2**) and Symmetric (**3**) Cyano-Stilbene Derivatives

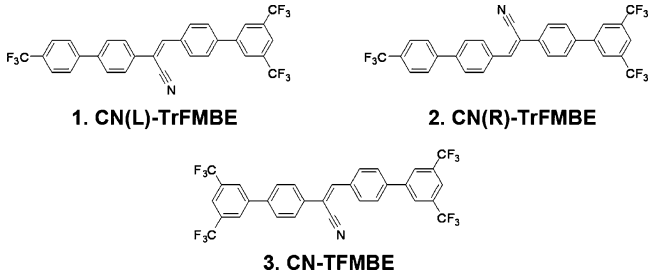

π-dimer stacking and its shear-induced displacement competing with [2 + 2] cycloaddition are responsible for the unique fluorescence behavior of the novel asymmetric AIEE compounds **1** and **2**. We have also demonstrated that the photo- and thermochemically addressable fluorescence changes in these novel AIEE compounds have a high contrast ratio and are reversible, which means that they are likely to have practical applications in optical memory systems.

Results and Discussion

The chemical structures of the newly designed and synthesized asymmetric cyano-stilbene derivatives **1** (CN(L)-TrFMBE) and **2** (CN(R)-TrFMBE) are shown in Scheme 1. These compounds were readily synthesized in only three steps according to Scheme S1 (Supporting Information) *via* Suzuki coupling and Knoevenagel reactions in good yields. They were characterized by ^{1}H NMR, ^{13}C NMR, mass spectroscopy, and elemental analysis (see the Supporting Information).

Interestingly, CN(L)-TrFMBE and CN(R)-TrFMBE exhibit an unusual fluorescence behavior that is different from that of the AIEE crystal of **3** (CN-TFMBE).[22] The latter compound is very highly fluorescent in the crystalline state but nonfluorescent in solution, i.e., it exhibits AIEE. In contrast, CN(L)-TrFMBE and CN(R)-TrFMBE, are virtually nonfluorescent in the crystal and solution states. Their crystals are easily obtained with recrystallization techniques because of their strong intermolecular interactions. Surprisingly, however, these nonfluorescent crystals were found to gradually become highly fluorescent with strong sky-blue emissions when they are exposed to prolonged irradiation from a hand-held UV light (1.2 mW·cm^{-2}), as shown in Figure 1a. The time-dependent evolutions of the fluorescence spectrum and absolute photoluminescence (PL) quantum efficiency (Φ_{PL}) of CN(L)-TrFMBE crystal were measured in real-time at an excitation wavelength of 365 nm and are respectively shown in b and c of Figure 1. It can be clearly seen that the intensity of the fluorescence emission in the solid state increases dramatically upon UV irradiation within several minutes, resulting in a fluorescence quantum yield as high as 0.24 (Figure 1c). This phenomenon was also observed for CN(R)-TrFMBE (Table 1 and Figure 1d).

To investigate the possible origin of this unexpected photochromic behavior,[29] we examined the morphological evolution of the crystal surfaces upon UV irradiation and the results are shown in Figure 2. Our optical microscopic observations revealed that there are distinct changes in the coloration and surface morphology of the irradiated crystals. In particular, the crystals became opaque with a color change from yellowish green to off-white upon UV irradiation. Moreover, the SEM images show deformations and large internal fractures on the surfaces of these crystals. As can be seen in panels 3 and 6 of Figure 2, the crystals of CN(L)-TrFMBE and CN(R)-TrFMBE have smooth and clear surfaces before UV irradiation, whereas there is extensive cracking and clefts in the crystal lattices after exposure to 365 nm UV light for 60 s. These morphological changes suggest that the fluorescence enhancement upon UV irradiation is probably caused by reconstructive phase transition[30] in either the molecular conformation or the stacking mode in the crystal state.[31]

Further, we observed that the fluorescence emission from CN(L)-TrFMBE and CN(R)-TrFMBE can also be switched on by a small external shear-strain. As shown in Figure 3, the initially nonfluorescent powdered crystal of CN(L)-TrFMBE immediately became highly fluorescent when it was briefly smeared with a spatula. The fluorescence turn-on only occurred at the smeared area, as indicated by a green arrow in the photograph in the inset in Figure 3a. A few examples of such pressure- or shear-induced fluorescence modulation have also very recently been reported for molecules that are structurally different from ours.[32−34] Although the detailed mechanism of shear-induced fluorescence modulation is still unclear and is likely to vary from case to case, it seems plausible that the mechanical force alters the molecular stacking rather than the chemical structure. In this context, we carried out a comprehensive crystal structure analysis and theoretical calculations to assess this mechanism (*vide infra*).

X-ray quality crystals of CN(L)-TrFMBE and CN(R)-TrFMBE were grown at room temperature with the solution diffusion technique[35] in a tetrahydrofuran (THF)/methanol (MeOH) system. Slow diffusion of THF solutions of CN(L)-TrFMBE or CN(R)-TrFMBE into MeOH resulted within a week in the greenish yellow crystals shown in a and b of Figure 2. Unfortunately, the crystal of CN(L)-TrFMBE decomposed gradually during the collection of reflections, probably due to its sensitivity to the light in the X-ray laboratory. For this reason, we rapidly collected the reflections in a relatively small θ range (2.08−20.51) in the dark. Although the rather poor crystal quality of both crystals reflects on the relatively large R values, their ORTEP drawings clearly show the overall molecular geometry with no doubt about the atom connectivity.

CN(L)-TrFMBE and CN(R)-TrFMBE are structural isomers due to the different positions of the central CN group. The molecular structure of CN(L)-TrFMBE is shown in Figure 4a.

(29) (a) Gavezzotti, A.; Simonetta, M. *Chem. Rev.* **1982**, *82*, 1–13. (b) Irie, M. *Chem. Rev.* **2000**, *100*, 1685–1716.
(30) (a) Garcia-Garibay, M. A. *Angew. Chem., Int. Ed.* **2007**, *46*, 8945. (b) Keating, A. E.; Garcia-Garibay, M. A. *Organic and Inorganic Photochemistry*; Marcel Dekker: New York, 1998; Vol. 2.
(31) (a) Turowska-Tyrk, I. *J. Phys. Org. Chem.* **2004**, *17*, 837–847. (b) Harris, K. D. M.; Thomas, J. M.; Williams, D. *J. Chem. Soc. Faraday Trans.* **1991**, *87*, 325–331. (c) Kaupp, G. *Angew. Chem., Int. Ed.* **1992**, *31*, 592–595. (d) Hasegawa, M. *Chem. Rev.* **1983**, *83*, 507–518. (e) Kuzmanich, G.; Natarajan, A.; Chin, K. K.; Veerman, M.; Mortko, C. J.; Garcia-Garibay, M. A. *J. Am. Chem. Soc.* **2008**, *130*, 1140–1141.
(32) (a) Kunzelman, J.; Kinami, M.; Crenshaw, B. R.; Protasiewicz, J. D.; Weder, C. *Adv. Mater.* **2008**, *20*, 119–122. (b) Sagara, Y.; Mutai, T.; Yoshikawa, I.; Araki, K. *J. Am. Chem. Soc.* **2007**, *129*, 1520–1521.
(33) (a) Mizuguchi, J.; Tanifuji, N.; Kobayashi, K. *J. Phys. Chem. B* **2003**, *107*, 12635–12638. (b) Ariga, K.; Terasaka, Y.; Sakai, D.; Tsuji, H.; Kikuchi, J. *J. Am. Chem. Soc.* **2000**, *122*, 7835–7836. (c) Yamamoto, T.; Muramatsu, Y.; Lee, B. L.; Kokubo, H.; Sasaki, S.; Hasegawa, M.; Yagi, T.; Kubota, K. *Chem. Mater.* **2003**, *15*, 4384–4393.
(34) (a) Mizobe, Y.; Ito, H.; Hisaki, I.; Miyata, M.; Hasegawa, Y.; Tohnai, N. *Chem. Commun.* **2006**, 2126–2128. (b) Mutai, T.; Satou, H.; Araki, K. *Nat. Mater.* **2005**, *4*, 685–687. (c) Davis, R.; Rath, N. P.; Das, S. *Chem. Commun.* **2004**, 74–75.
(35) Jones, P. G. *Chem. Br.* **1981**, *17*, 222–224.

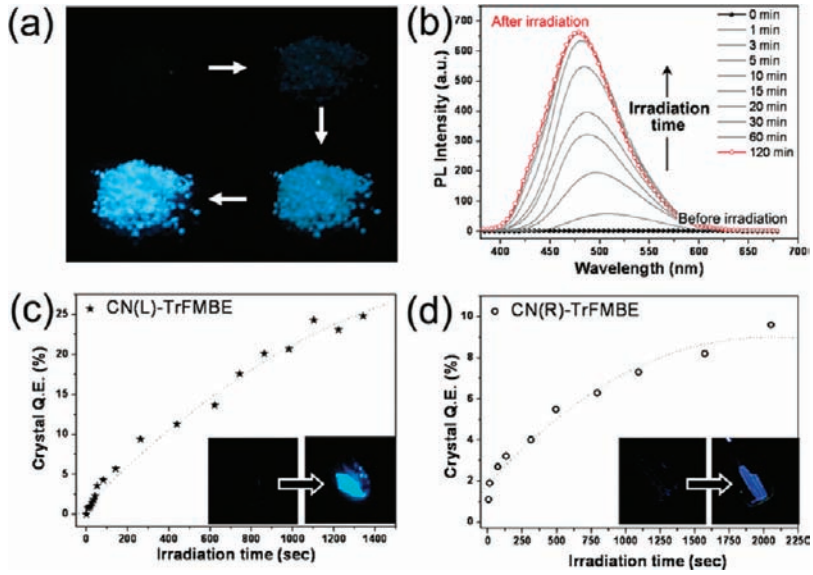

Figure 1. (a) Fluorescence images of powdered CN(L)-TrFMBE crystal for various UV irradiation times (0, 1, 5, and 30 min). (b) Fluorescence spectra (λ_{ext} = 365 nm) of CN(L)-TrFMBE bulk crystals on a quartz plate. (c) Absolute PL quantum efficiencies (Φ_{PL}) of CN(L)-TrFMBE and (d) CN(R)-TrFMBE as functions of irradiation time. The photographs in the insets show fluorescence images of large single crystals before and after irradiation.

Table 1. Optical Properties and ^{1}H NMR Assignments of the Monomers and σ-Dimers of CN(L)-TrFMBE and CN(R)-TrFMBE

compound	UV/vis spectroscopy[a] λ_{max} (nm)	PL spectroscopy[a] λ_{max} (nm)	FT-IR[b] IR (cm^{-1})	^{1}H NMR[c] $H_{olefine}$ (δ)/$H_{aromatic}$ (δ)	H_{cycl} (δ)/$H_{aromatic}$ (δ)	$\Phi_{m\rightarrow de}$[d] (%)
CN(L)-TrFMBE	345	441	2217	7.67/7.74−8.07		90 ± 5
σ-dimer of CN(L)-TrFMBE	265	314	2234		5.39/7.46−7.99	
CN(R)-TrFMBE	347	436	2220	7.67/7.72−8.05		85 ± 5
σ-dimer of CN(R)-TrFMBE	265	311	2234		5.38/7.43−8.05	

[a] 2×10^{-5} mol·L^{-1} in tetrahydrofuran (THF). [b] In KBr pellets. [c] In $CDCl_3$. [d] The ratio of products obtained after conversion of the reactant based on the integration of the product peaks in the ^{1}H NMR and HPLC spectra. Irradiation was carried out for 120 min using a 365 nm hand-held UV lamp (1.2 mW·cm^{-2}) under atmospheric conditions at room temperature.

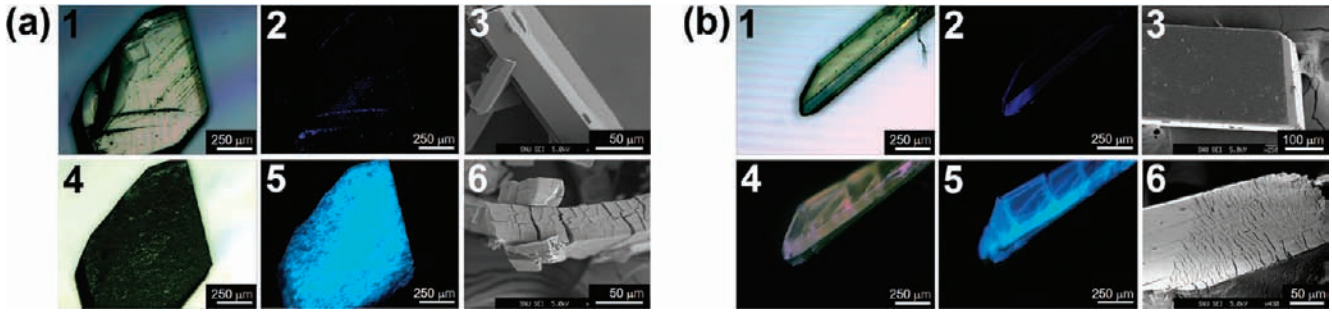

Figure 2. Optical and fluorescence images of single crystals of CN(L)-TrFMBE (a) and CN(R)-TrFMBE (b) before irradiation (1, 2) and after irradiation (4, 5) with 365 nm UV light for 60 s. SEM photographs of the powdered crystals before (3) and after (6) irradiation.

All four rings are significantly twisted from each other: one pair (C2−C7; C8−C13) with a dihedral angle of 30.8(4)° and the other pair (C17−C22 and C23−C28) with that of 36.6(3)°. The molecular structure of CN(R)-TrFMBE is presented in Figure 4b, which also shows significantly twisted rings: one pair (C2−C7; C8−C13) with a dihedral angle of 33.0(2)° and the other pair (C17−C22 and C23−C28) with that of 34.6(2)°. It is worth noting that the torsion angles of C4−C5−C8−C9 and C19−C20−C23−C24 in CN(L)-TrFMBE are 30(1) and −35(1)°, respectively, whereas those in CN(R)-TrFMBE are −31(1) and 34(1)°. These torsion angles suggest that both structures are related in terms of conformation. If we put the central fragment {−C_6H_4−C(CN)−CH−(−C_6H_4)} of both compounds in the same orientation, we can readily recognize the relative orientations of the terminal groups (C_6H_4−CF_3 and C_6H−$(CF_3)_2$) with respect to the central fragment. The terminal groups in CN(L)-TrFMBE can go to the corresponding groups in CN(R)-TrFMBE by counterclockwise rotating the C_6H_4−CF_3 fragment by 61° (with respect to the central moiety) and the C_6H_3-$(CF_3)_2$ fragment by 69°. This phenomenon can be vividly illustrated by the space-filling moles of both structures with respect to the central fragment (Figure S4 in the Supporting Information).

The most significant structural feature of CN(L)-TrFMBE and CN(R)-TrFMBE shown in Figure 4 is the presence of antiparallel *π-dimers* (also known as head-to-tail (HT) *π-dimers*[6]), which comprise very close pairs of stilbenic C=C bonds with center-to-center distances of 3.785 (Figure 4c) and 3.889 Å (Figure 4d). It is evident from the *π-dimer* geometries shown in Figure 4 that the three asymmetrically substituted CF_3 units

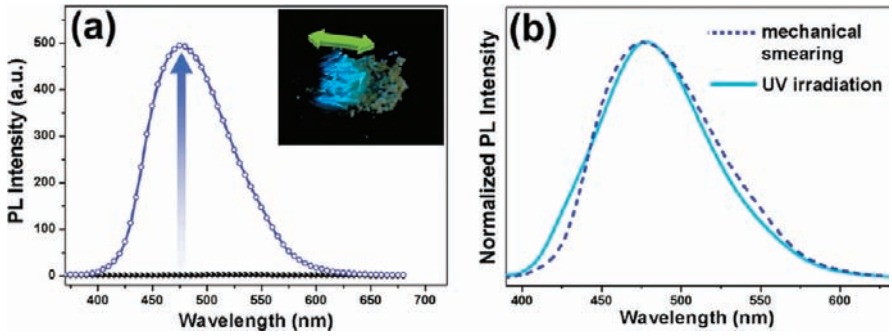

Figure 3. (a) Fluorescence turn-on of a powdered CN(L)-TrFMBE crystal on a quartz plate after smearing with a metal spatula. The inset shows a fluorescence image of the powdered crystals on a quartz plate. The green arrow indicates the area smeared with the spatula. (b) Normalized PL spectra after mechanical smearing (blue dashed line) and UV irradiation (sky-blue line).

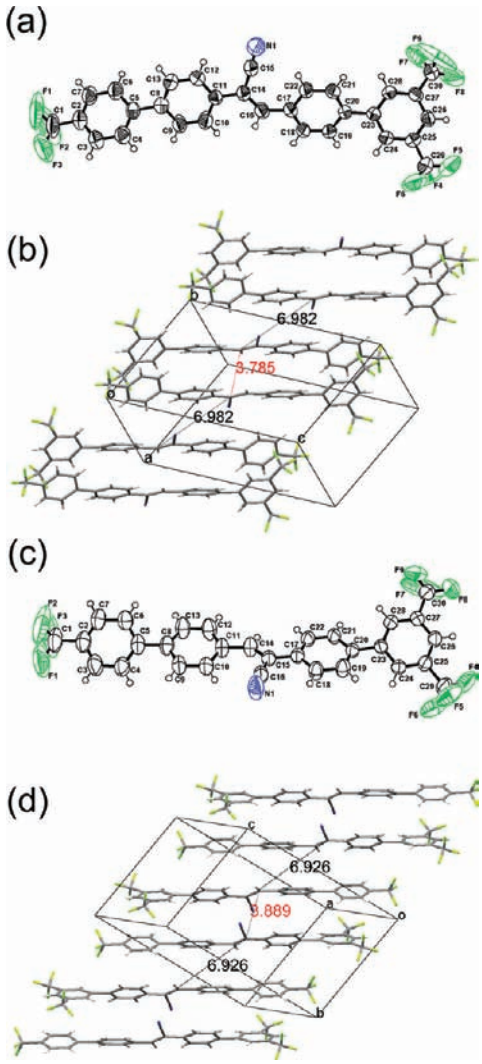

Figure 4. X-ray crystallography of single crystals of the asymmetric cyano-stilbene derivatives: ORTEP drawings of CN(L)-TrFMBE (a) and CN(R)-TrFMBE (c) with 50% probability thermal ellipsoids. The center-to-center distances between the stilbenic double bonds in the π-dimers are 3.785 Å (b) and 3.889 Å (d) respectively.

are the key elements of antiparallel *π-dimer* formation because of the resulting C−F···H−C and C−F···π interactions[16] in addition to the favorable $\pi-\pi$ and dipolar interactions. The pair of molecules in the antiparallel *π-dimer* are related by a center of symmetry and maintain close contact to enable [2 + 2] cycloaddition. For the topochemical [2 + 2] cycloaddition

Table 2. Crystallographic Details of the Asymmetric Cyano-Stilbene Derivatives[a]

	CN(L)-TrFMBE	CN(R)-TrFMBE
empirical formula	$C_{30}H_{16}F_9N$	$C_{30}H_{16}F_9N$
fw	561.44	561.44
temperature, K	293(2)	293(2)
crystal system	triclinic	triclinic
space group	$P\bar{1}$	$P\bar{1}$
a, Å	8.7256(3)	8.626(2)
b, Å	10.1686(4)	10.283(2)
c, Å	15.1679(5)	15.342(4)
α, deg	74.382(2)	75.91(2)
β, deg	81.966(2)	79.12(2)
γ, deg	84.065(2)	82.83(2)
V, Å	1280.34(8)	1291.7(5)
Z	2	2
d_{cal}, g cm^{-3}	1.456	1.443
μ, mm^{-1}	0.131	0.13
F (000)	568	568
θ range (deg)	2.08−20.51	2.05−25.00
no. of reflns measured	11180	4805
no. of reflns unique	2564	4487
no. of reflns with $I > 2\sigma(I)$	2084	3164
no. of params refined	361	362
max., in $\Delta\rho$(e Å^{-3})	0.723	0.655
min., in $\Delta\rho$(e Å^{-3})	−0.498	−0.427
GOF on F^2	1.086	1.09
distance of center-to-center (Å)	3.798	3.889
R^b	0.1131	0.1053
wR2[c]	0.3149	0.3167

[a] Single crystals of these compounds were grown at room temperature by using the solution diffusion technique within a tetrahydrofuran (THF)/methanol (MeOH) system. [b] $R = \Sigma[|F_o| - |F_c|]/\Sigma|F_o|]$. [c] wR2 $= \Sigma[w(F_o^2 - F_c^2)^2]/\Sigma[w(F_o^2)^2]^{1/2}$.

reaction to occur in the crystalline state, it is known that the center-to-center distance between the reactive double bonds should be less than 4.2 Å[6] and that there should be a high degree of overlap between the π-orbitals of the reactive partners, which is determined by the geometrical parameters θ_1, θ_2, θ_3, and *d*,[5−8] with ideal values of 0, 90, 90°, and 0 Å, respectively. The crystallographic parameters of CN(L)-TrFMBE and CN(R)-TrFMBE are summarized in Table 2 and depicted in Figures 4 and S2,S3 (see the Supporting Information).

These parameters indicate that the antiparallel *π-dimers* have [2 + 2] cycloaddition reactivity: the actual values of the center-to-center distance, θ_1, θ_2, θ_3, and *d* are 3.785 Å, 0°, 101.95°, 84.51°, and 0.784 Å for CN(L)-TrFMBE, and 3.889 Å, 0°, 113.69°, 89.40°, and 1.563 Å for CN(R)-TrFMBE. Therefore, it is expected that the initial antiparallel *π-dimers* will be transformed into covalently bonded '*σ-dimer* ([2 + 2] cycloadducts)' *via* [2 + 2] cycloaddition when the crystals are

illuminated with UV light. This expectation is consistent with the initial nonfluorescent state of the single crystals and also the crystal cracking visible in Figure 2. The rationale for the former observation is that the absorbed UV photon contributes exclusively to the [2 + 2] cycloaddition rather than photoluminescence generation. The volume of the *σ-dimer* is larger than that of the *π-dimer*, which explains the latter observation. The remaining puzzle is then why the photoluminescence increases with both prolonged UV irradiation or an external shearing action.

The shear-induced emission (SIE) observed in Figure 3 suggests that the fluorescence "turn-on" is probably associated with the shear-induced displacement of the *π-dimer* pair, which increases the rate of photoluminescence at the cost of frustrated [2 + 2] cycloaddition. As for the prolonged UV irradiation effect, perhaps the same process occurs due to the 'internal shear force' generated by the expanding volume of the *σ-dimer*. We carried out comprehensive structural, optical, and crystallographic analyses to assess this idea, as described below.

The pure *σ-dimers* were obtained in high yield by carrying out UV irradiation for 3 h. The remaining monomer was removed with column purification and recrystallization from MeOH. The resulting materials were then characterized with ^{1}H NMR, FT-IR, HPLC, mass spectroscopy, and DSC analysis. These data are in good agreement with data reported for other *σ-dimer* systems.[7a] In the ^{1}H NMR spectrum of the CN(L)-TrFMBE monomer, the vinylic protons of the monomer resonate in the range at δ 8.08−7.66 ppm mingled with aromatic protons. These monomer signals (red arrow, top of Figure 5a) are not present, however, in the spectrum of the *σ-dimer*, which contains a characteristic singlet at δ 5.39 ppm (red arrow, bottom of Figure 5a) due to the cyano-substituted cyclobutane ring. The longer wavelength band (at 345 nm) due to stilbenic conjugation in the monomer is completely absent from the UV/vis absorption spectrum of the *σ-dimer*, and there is a much shorter wavelength band characteristic of the *σ-dimer* at 265 nm (Figure 5b). Accordingly, the color of the *σ-dimer* is off-white, as shown in Figure 6a, in contrast to the yellowish green color of the monomer. The fluorescence emission spectra of the monomer and the *σ-dimer* of CN(L)-TrFMBE in THF solution are shown in Figure 5b. The monomer is barely fluorescent in solution (*note that this behavior is similar to that of other AIEE dyes like CN-TFMBE*[22]) with an emission maximum at 441 nm, whereas the CN(L)-TrFMBE *σ-dimer* exhibits very weak emission centered around 314 nm when excited at 265 nm, which is attributed to the biphenyl unit in the *σ-dimer*. Consequently, the exceptionally strong 478 nm emission from the UV-irradiated crystal shown in Figure 1 does not come from the photoproduced *σ-dimer*, but from other species influenced by the [2 + 2] cycloaddition. The optical properties and ^{1}H NMR assignments of the monomer and *σ-dimer* are summarized in Table 1.

In the course of the topochemical [2 + 2] cycloaddition of the *π-dimer*, it is most probable that the formation of the sterically bulkier *σ-dimer* results in strain and pressure in the crystalline lattice that exerts an internal shear-force on the neighboring *π-dimer* pair. Shear-induced deformation of the *π-dimer*, including changes in the center-to-center distance and other geometrical features required for [2 + 2] cycloaddition,[5−8] then results in fluorescence turn-on at the cost of frustrated [2 + 2] cycloaddition. This idea is supported by the identical effects of external shear force and UV irradiation on the photoluminescence turn-on, as shown in Figure 3b, and also by the crystal

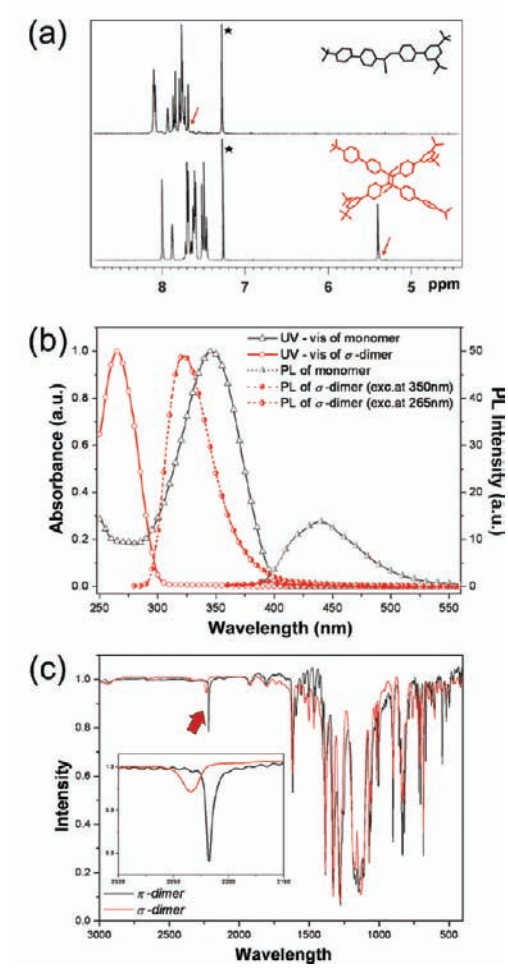

Figure 5. Results for the CN(L)-TrFMBE monomer and the *σ*-dimer: (a) ^{1}H NMR spectra of the monomer (above) and the *σ*-dimer (below) in $CDCl_3$ at room temperature; (b) UV/vis absorption spectra (open symbols) and PL spectra (filled symbols) of the monomer (triangles) and the *σ*-dimer (circles); (c) FT-IR absorption spectra (KBr pellets) of the *π*-dimer (monomer) and the *σ*-dimer. The inset and the red arrow show the nitrile stretching peaks of the *π*-dimer and the *σ*-dimer.

cracking upon UV irradiation shown in Figure 2. Further, the degree of crystallinity decreases after UV irradiation, as shown by powder X-ray diffraction measurements (see the Supporting Information, Figure S1).

If the fluorescence is turned on according to this mechanism, there should remain a finite amount of emitting CN(L)-TrFMBE monomer (deformed *π-dimer* incapable of cycloaddition) in the crystal after UV illumination. To clarify this point, we monitored the evolution of the chemical structure of the crystal as a function of UV irradiation time by using ^{1}H NMR, UV/vis absorption, and HPLC. To ensure complete topochemical [2 + 2] cycloaddition, we irradiated the powdered CN(L)-TrFMBE crystal for as long as 2 h; i.e. we took into account the fluorescence saturation behavior shown in Figure 1. As expected from the very favorable crystal structure (*vide supra,* Figure 4 and related discussion), [2 + 2] cycloaddition proceeds efficiently in the crystalline phase. Figure 7a shows the ^{1}H NMR spectra for CN(L)-TrFMBE and the *σ-dimer* recorded after various irradiation times at room temperature. The spectrum at the top of Figure 7a is for the parent, CN(L)-TrFMBE, prior to irradiation. As the [2 + 2] cycloaddition proceeds, the corresponding intensities of the vinyl proton signal (inverted triangles) assigned to the monomer decrease with a gradual increase in

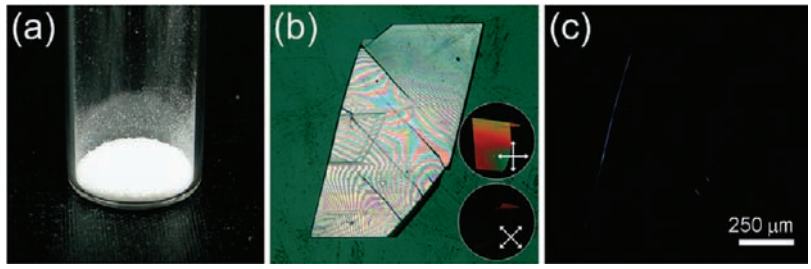

Figure 6. (a) Photograph of pure *σ-dimer* powder of CN(L)-TrFMBE after column purification. (b) Optical microscopy image (the circled inset photographs show the birefringence under crossed polarizers) and (c) fluorescence microscopy (under 365 nm UV light) image pure *σ-dimer* of the CN(L)-TrFMBE, obtained by using column purification and recrystallization.

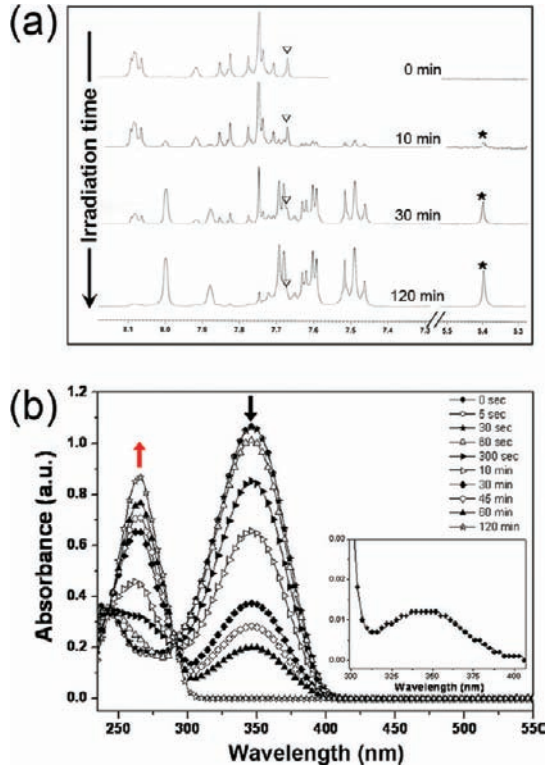

Figure 7. Fluorescence enhancement as the result of an internal shear force *via* [2 + 2] cycloaddition. ^{1}H NMR and UV/vis absorption spectra for the conversion of monomer to *σ*-dimer in the solid state as a result of irradiation with 365 nm hand-held UV light (1.2 mW·cm^{-2}) at 25 °C: (a) ^{1}H NMR spectra after various irradiation times (0 to 2 h, vinyl protons (▽) and protons of the cyclobutane ring (*)); (b) UV/vis absorption spectra of CN(L)-TrFMBE powdered crystal recorded in THF (2×10^{-5} mol·L^{-1}). The inset shows the absorption band of the monomer remaining after irradiation. The black arrow indicates the decrease in the signal intensity of the monomer on irradiation for 0 to 2 h. The inset shows the absorption spectrum of the remaining monomer (after 2 h, black circles).

the intensity of the new proton signals (stars) due to the cyclobutane ring, which indicates the concomitant formation of a [2 + 2] cycloadduct. The bottom of Figure 7a indicates almost complete conversion to the *σ-dimer*, with only a small amount of emitting CN(L)-TrFMBE monomer possibly remaining. The proportion of the remaining monomer was determined from the integration of the proton peaks in the ^{1}H NMR spectra to be approximately 5%. This value is in good agreement with that obtained from HPLC analysis (see the Supporting Information, Figure S5).

In addition, the presence of the emitting CN(L)-TrFMBE monomer, i.e., the sheared/displaced monomer pair immune to [2 + 2] cycloaddition and generated by *σ-dimer* formation in its neighborhood, was further confirmed with spectroscopic analysis. Powdered crystals of CN(L)-TrFMBE were irradiated with UV for varying durations and then dissolved in THF for the recording of their UV/vis absorption spectra. As shown in Figure 7b, the intensity of the absorption peak of the CN(L)-TrFMBE monomer at 345 nm (black arrow) gradually decreases with increasing UV irradiation time, whereas that of the *σ-dimer* (red arrow) at 265 nm increases simultaneously. Note that the latter peak exactly matches the absorption maximum wavelength of the purified *σ-dimer* compound (Figure 5b). Importantly, the presence of the emitting CN(L)-TrFMBE monomer, i.e., the sheared/displaced monomer pair immune to [2 + 2] cycloaddition, can be confirmed from the remaining monomer emission (see the inset in Figure 7b) after prolonged UV irradiation for 2 h. All these experimental results support our proposed mechanism: the turn-on fluorescence in solid-state is attributed to SIE through the molecular displacement frustrated [2 + 2] cycloaddition, which favors activation of radiative decay to the ground state.

In order to further investigate the fluorescence turn-on mechanism, we carried out quantum chemical calculations based on density functional theory (DFT, B3LYP/6-31G** level implemented with Gaussian 03[36]) with particular emphasis on the electronic interactions within the crystals upon optical excitation. The geometries of the antiparallel *π-dimers* were extracted from the crystal structures. The geometries of the *σ-dimer* and a single molecule (isolated state) of CN(L)-TrFMBE were subjected to iterative optimization to determine the low-energy structures. In addition, the geometries of 10 singlet states were calculated using the time-dependent DFT (TD-DFT, B3LYP/6-31G**) method; the first and second singlet excited states are shown in Figure 8. The isolated single molecule has a well-defined highest occupied molecular orbital (HOMO) and a well-defined lowest unoccupied molecular orbital (LUMO), which result in benzenoid and quinoid isodensity plots respectively. The corresponding first singlet excited state has an excitation energy of 3.26 eV, which is in good agreement with the observed $\pi-\pi^*$ transition band in the absorption spectrum (345 nm, Figure 5b). An interesting result is that greater stabilization of the excited states is predicted for the *π-dimer* than for the isolated state: the respective stabilization energies are 0.25 eV for state S_1 and 0.76 eV for state S_2. This difference is due to the prominent in-phase interaction between the LUMOs of the two molecules in the *π-dimer*. As shown schematically in Figure 8, this interaction significantly distorts the shape of the LUMO and finally results in an intermolecular bonding interaction. Note also that the geometric position of this bonding interaction coincides with that of the [2 + 2]

(36) Frisch, M. J.; et al. *Gaussian 03* Gaussian, Inc.: Wallingford CT, 2004.

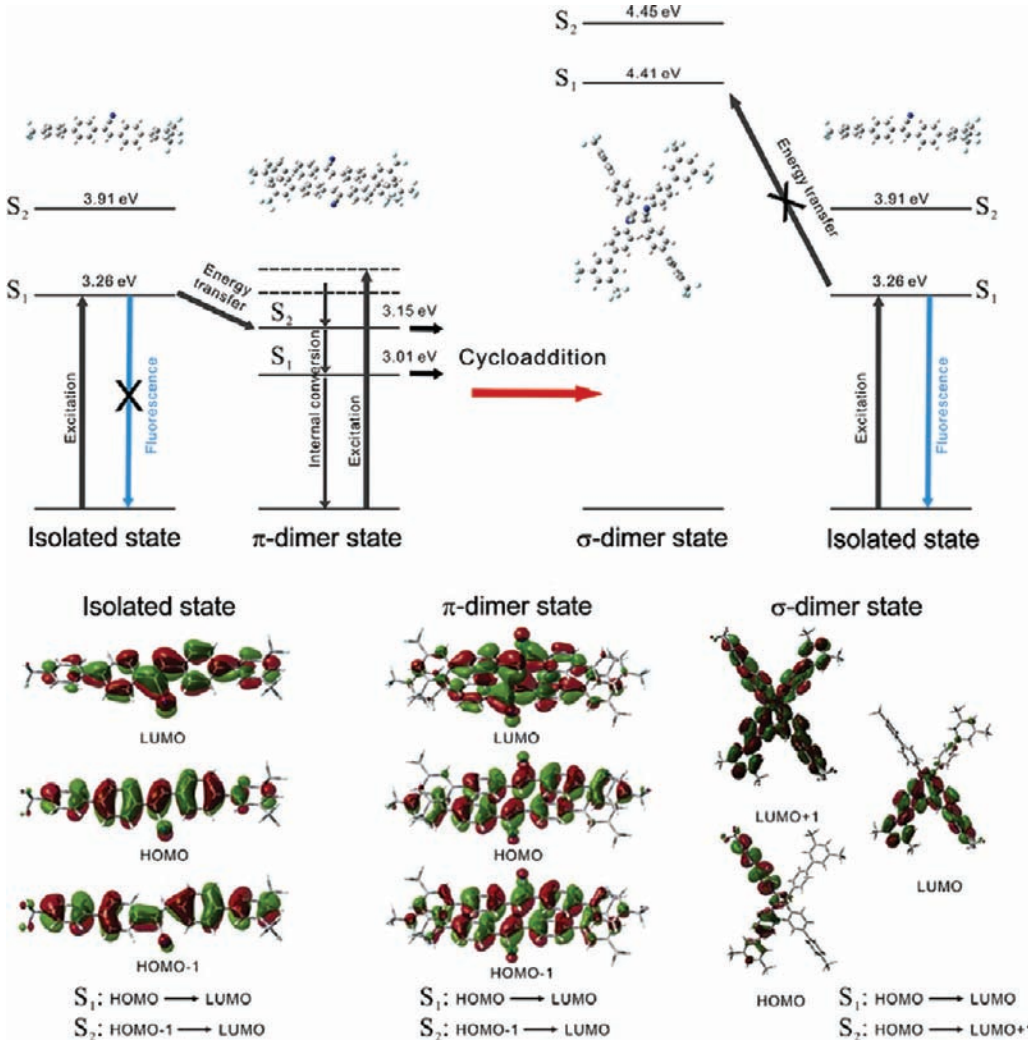

Figure 8. Proposed mechanism for the shear-induced emission of asymmetric cyano-stilbene in the solid state.

cycloaddition, as discussed above. In contrast, the S_1 and S_2 states of the *σ-dimer* are predicted to have energies that are 1.15 and 0.54 eV higher, respectively, than those of the isolated state. This result makes sense because the intramolecular conjugative plane is disconnected at the ex-cyanovinyl position.

The results of these calculations support our mechanism for the enhanced fluorescence and the photochemical [2 + 2] cycloaddition in the solid state. In the well-ordered crystalline state containing *π-dimer* pairs, once the CN(L)-TrFMBE molecule is optically excited, two different photophysical pathways are available: a nonradiative [2 + 2] cycloaddition with the *π-dimer* partner, and a radiative fluorescent transition. Since virtually no fluorescence is observed during the initial stages of irradiation, the former pathway is preferred, resulting in the high-energy *σ-dimer* which cannot accept the excited-state energy exothermically. In addition, during the [2 + 2] cycloaddition process, the *π-dimer* state plays the role of an energy sink that blocks the fluorescing radiative decay of the excited molecule. However, as irradiation and the formation of the *σ-dimer* progresses, shear-displaced CN(L)-TrFMBE molecules are gradually generated and the *π-dimer* energy sink is removed, which results in enhanced fluorescence emission.

With fluorescence switching applications in mind, we investigated the stability and reversibility of the [2 + 2] cycloaddition and the relevant fluorescence changes. The shear-induced and UV-induced "turn-on" states of the CN(L/R)-TrFMBEs were found to be stable for over 1 year if stored even under atmospheric conditions. It was also found that thermal heating of the irradiated powder to melting temperature (240 °C) fully restores the original "turn-off" state due to the thermal dissociation of the cyclobutane ring,[37] which regenerates the pure nonfluorescent powdered crystal with *π-dimer* stacking. We also confirmed the structure of the restored *π-dimer* and the total disappearance of the *σ-dimer* by using ^{1}H NMR, mass spectroscopy, and UV/vis absorption spectroscopy. As shown in Figure 9a, there is a strong endothermic peak at 193 °C in the DSC analysis of the *σ-dimer* due to cyclobutane ring dissociation, which generates in CN(L)-TrFMBE monomers. To directly monitor the recovery of *π-dimer* stacking from the *σ-dimer*, X-ray diffraction (XRD) patterns of powder crystal samples at three different treatment stages (before and after UV irradiation and subsequent thermal heating) have been measured and compared from each other (see Figure S6 in the Supporting Information). On irradiation, the characteristic diffraction peaks (black arrows in Figure S6) attributed to the well-ordered *π*-dimer packing disappeared, remaining no sharp signal behind (gray line in Figure S6). After a subsequent thermal heating,

(37) Novak, K.; Enkelmann, V.; Wegner, G.; Wagener, K. B. *Angew. Chem., Int. Ed.* **1993**, *32*, 1614–1616.

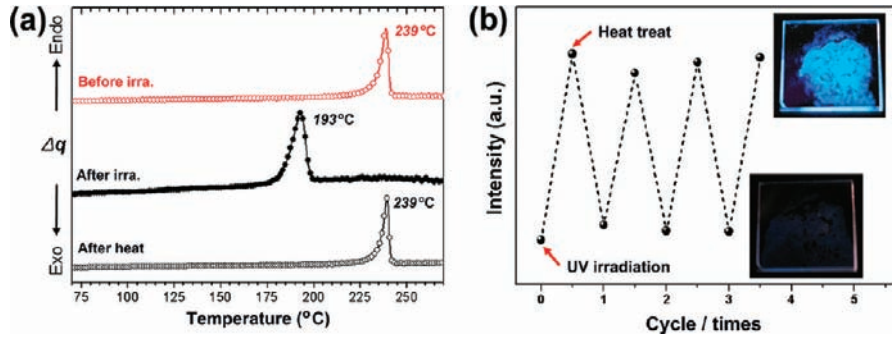

Figure 9. (a) DSC curves showing the thermal transition of the CN(L)-TrFMBE monomer (before irradiation, red open circles), *σ*-dimer (after irradiation, filled circles), and monomer (after thermal heating, black open circles) obtained with a heating rate of 10 °C/min. (b) This fluorescence modulation spectrum shows the reversibility of the PL intensity of the *π*-dimer packing mode and the irradiated states. The photographs in the insets show the fluorescence emission of the turn-on and turn-off states of CN(L)-TrFMBE.

however, it is clearly noted that the original peaks of the monomer (*π-dimer* packing) were restored to show sharp characteristic peaks again (sky-blue line in Figure S6). The XRD patterns of CN(L)-TrFMBE before UV irradiation as well as after thermal heating comprise the peaks of the single crystal CN(L)-TrFMBE, although the crystallinity of the powdered crystals is not likely to be very high. All these data strongly support a reversible switching between the nonfluorescent *π-dimer* and the fluorescent mixed *σ-dimer* states via UV/shear and heating (Figure 9b).

Conclusion

We have designed and synthesized asymmetric cyano-stilbene derivatives containing trifluoromethyl ($-CF_3$) substituents that exhibited unique shear- and/or UV-induced fluorescence turn-on with reversible switching manner *via* thermal treatment. Based on structural, optical, and DFT studies, we found that these crystals contain *π-dimer* molecular pairs with a strong tendency to [2 + 2] cycloaddition, which results in the formation of volume-expanded *σ-dimers* on irradiation with UV light. The shear- and/or UV-induced fluorescence turn-on can be explained in terms of the lateral displacement of the *π-dimer* molecular pairs, which results in enhanced fluorescence emission at the cost of frustrated [2 + 2] cycloaddition.

Experimental Section

General Considerations. Starting materials were purchased from Alfa Aesar Co. and Sigma Aldrich Chemical Co. and used without further purification unless otherwise stated. The synthetic routes and characterizations of CN(L)-TrFMBE and CN(R)-TrFMBE are described in the Supporting Information. UV/vis absorption spectra were recorded on a Shimadzu UV-1650 PC spectrometer using samples in solution. Fluorescence spectra were recorded on a Shimadzu RF 5301 PC fluorescence spectrometer using samples in the solution or solid state. The absolute photoluminescence quantum efficiency (Φ_{PL}) of the crystal was measured using an integrating sphere (Labsphere Co., 600 diameter) as described in ref 38. A continuous wave Xe-lamp (500 W, Melles Griot Co.) was used as the excitation light source, and a monochromator (Acton Research Co.) attached to a photomultiplier tube (Hamamatsu) was used as the optical detector system. All of the systems were calibrated using a tungsten−halogen standard lamp and deuterium lamp (Ocean Optics LS-1-CAL and DH-2000-CAL, respectively). Φ_{PL} was calculated based on the de Mello method.[38] ^{1}H NMR spectra were recorded on DPX Bruker 300 (300 MHz) and Bruker Avance 500 (500 MHz) spectrometers. All NMR spectra were referenced to the solvent. ^{13}C NMR spectra were also measured. Proton (0.1 ppm) chemical shifts were measured with respect to internal TMS in $CDCl_3$. ^{13}C chemical shifts were reported in ppm relative to $CDCl_3$. TLC analyses were carried out on aluminum sheets coated with silica gel 60 (Merck 5554). Column chromatography was performed on Merck silicagel 60. Mass spectra were measured using a JEOL, JMS AX505WA mass spectrometer. Elemental analysis was carried out using a CE instruments, EA110 elemental analyzer. SAXS measurements were performed using a Bruker GADDS equipped with a 2D area detector, operating at 3 kW. Differential scanning calorimetry (DSC) was performed on a Perkin-Elmer DSC7 instrument at a heating rate of 10 °C min^{-1}. High performance liquid chromatography (HPLC) measurements were carried out using a Shimadzu LC-20AD chromatograph with an injection volume of 1 μm. Field emission scanning electron microscopy (FE-SEM) images were obtained with a JSM-6330F (JEOL) FE-SEM at an acceleration voltage of 12 kV, after sputter deposition of a thin conductive platinum coating onto the films.

Irradiation Procedure. The *π-dimer* finely powdered crystal and single crystal samples of CN(L)-TrFMBE and CN(R)-TrFMBE, placed at a distance of ~10 cm from the 365 nm hand-held UV lamp (1.2 mW·cm^{-2}) under atmospheric conditions at room temperature, were irradiated simultaneously for 3 h. Irradiation was continued until there was no further increase in product formation. The progress of the reaction was monitored by ^{1}H NMR. After irradiation, the *π-dimers* were purified by column chromatography over silica gel and recrystallization from MeOH.

Optical Properties. The asymmetric compounds were irradiated in the solid state. After irradiation, the powdered crystal was dissolved in THF and the spectrophotometric analysis was carried out.

X-ray Crystallography or Crystal Structure Determination. Single crystals of all the CN(L)-TrFMBE or CN(R)-TrFMBE compounds were obtained by dissolving the compounds (200 mg) in a minimum quantity of tetrahydrofuran (10 mL), followed by addition of methanol (20 mL) from the edges of the glass tube (radius of 20 mm). The glass tube was sealed and covered with black paper without disturbing the solvent layers and was kept in a dark place. The resulting crystals were washed several times with methanol and dried under vacuum. All X-ray data were collected using a Siemens P4 diffractometer equipped with a Mo X-ray tube. No absorption corrections were made. All calculations were carried out using SHELXTL programs. The structure was solved by direct methods. All non-hydrogen atoms were refined anisotropically. All hydrogen atoms were generated in ideal positions and refined in a riding mode. Details on the crystal data, intensity collection, and refinement are given in Table 2. Crystallographic data for structures reported in this paper have been deposited as CIF files into the Cambridge Crystallographic Data Center as supplementary publication numbers CCDC 689876 and 689877.

(38) (a) Pålsson, L.-O.; Monkman, A. P. *Adv. Mater.* **2002**, *14*, 757–758. (b) de Mello, J. C.; Wittmann, H. F.; Friend, R. H. *Adv. Mater.* **1997**, *9*, 230–232.

Acknowledgment. This work was supported by the Korea Science and Engineering Foundation (KOSEF) through the National Research Laboratory Program funded by the Ministry of Science and Technology (No.2006-03246).

Supporting Information Available: Complete ref 36; full experimental section, including description of synthesis of CN(L)-TrFMBE, CN(R)-TrFMBE with complete spectral characterization data (^{1}H, ^{13}C NMR, mass, and elementary analysis date) and XRD data; complete crystallographic data (CIF files) of CN(L)-TrFMBE and CN(R)-TrFMBE. This material is available free of charge via the Internet at http://pubs.acs.org.

JA900803D